NMR paramagnetic relaxation due to the $S=5/2$ complex, Fe(III)-(*tetra-p*-sulfonatophenyl)porphyrin: Central role of the tetragonal fourth-order zero-field splitting interaction

Nathaniel Schaefle and Robert Sharp[a)]
Department of Chemistry, The University of Michigan, Ann Arbor, Michigan 48109

(Received 5 January 2005; accepted 15 February 2005; published online 6 May 2005)

The metalloporphyrins, Me-TSPP [Me=Cr(III), Mn(III), Mn(II), Fe(III), and TSPP=*meso*-(tetra-*p*-sulfonatophenyl)porphyrin], which possess electron spins $S=3/2$, 2, $5/2$, and $5/2$, respectively, comprise an important series of model systems for mechanistic studies of NMR paramagnetic relaxation enhancement (NMR-PRE). For these $S>1/2$ spin systems, the NMR-PRE depends critically on the detailed form of the zero-field splitting (zfs) tensor. We report the results of experimental and theoretical studies of the NMR relaxation mechanism associated with Fe(III)-TSPP, a spin $5/2$ complex for which the overall zfs is relatively large ($D\approx 10\ \mathrm{cm}^{-1}$). A comparison of experimental data with spin dynamics simulations shows that the primary determinant of the shape of the magnetic relaxation dispersion profile of the water proton R_1 is the tetragonal fourth-order component of the zfs tensor. The relaxation mechanism, which has not previously been described, is a consequence of zfs-induced mixing of the spin eigenfunctions of adjacent Kramers doublets. We have also investigated the magnetic-field dependence of electron-spin relaxation for $S=5/2$ in the presence of a large zfs, such as occurs in Fe(III)-TSPP. Calculations show that field dependence of this kind is suppressed in the vicinity of the zfs limit, in agreement with observation. © *2005 American Institute of Physics*. [DOI: 10.1063/1.1886748]

I. INTRODUCTION

The metalloporphyrins, Me-TSPP [Me=Cr^{III}, Mn^{III}, Mn^{II}, Fe^{III}, and TSPP=*meso*-(tetra-*p*-sulfonatophenyl)porphyrin, see Fig. 1], are water-soluble paramagnetic complexes with electron spins, $S=3/2$, 2, $5/2$, and $5/2$, respectively. These complexes are important model systems for mechanistic studies of NMR paramagnetic relaxation enhancement (NMR-PRE). For electron spins, $S>1/2$, the NMR-PRE depends on the detailed form of the form of the electron-spin Hamiltonian, which in porphyrin complexes is relatively simple because of physical and chemical constraints imposed by the four-fold site symmetry of the metal ion. In particular, the unique axis of the zero-field splitting (zfs) tensor coincides with the four-fold rotation axis, and orthorhombic zfs tensor components vanish; only the axial components of the zfs tensor (D and B_4^0) plus, for $S\geqslant 2$, a tetragonal fourth-order component (B_4^4) are nonzero. This study concerns the relaxation mechanism for Fe(III)-TSPP, an $S=5/2$ complex with a relatively large zfs ($D\approx 10\ \mathrm{cm}^{-1}$). We show below that the physical mechanism of the NMR-PRE depends critically on the tetragonal fourth-order zfs tensor component, B_4^4.

We report new magnetic relaxation dispersion (MRD) measurements for aqueous samples of Fe(III)-TSPP. (MRD refers to the profile of a NMR R_1 or R_2 relaxation rate measured as a function of laboratory magnetic-field strength; usually—as in the experiments described here—for the solvent water proton resonance at Zeeman field strengths, $B_0\leqslant 2$ T.) To provide a framework for interpreting the experimental data, we have carried out a series of model calculations, which explore the influence of each nonvanishing zfs tensor component, both quadratic and fourth order, on the form of the MRD profile. The experimental and theoretical results, taken together, lead to the conclusion that the primary determinant of the form of the MRD profile for this spin system (i.e., for $S=5/2$ with a large D parameter) is the ratio (B_4^4/D), where D is the quadratic cylindrical zfs parameter of ESR spectroscopy. The central role of the B_4^4 term in the relaxation mechanism of a Kramers spin system has not previously been recognized.

In prior work,[1,2] we have characterized NMR relaxation in the $S=2$ complex, Mn(III)-TSPP. For this non-Kramers spin system, the properties of the MRD profile are likewise determined principally by the tetragonal fourth-order zfs component, although the role of B_4^4 in the relaxation mechanism is entirely different physically for $S=2$ than for $S=5/2$. For $S=2$, the influence on the NMR-PRE results from a small B_4^4-induced splitting of the $m_S=\pm 2$ non-Kramers doublet, while for $S=5/2$, it results from B_4^4-induced mixing of the $m_S=\pm 3/2$ and $\mp 5/2$ spin eigenfunctions. For both the Kramers and non-Kramers spin systems, the axial quadratic zfs term, D, while an order of magnitude larger than B_4^4, has little influence on the properties of the MRD profile as long as the spin system remains in the vicinity of the zfs limit [i.e., as long as the largest zfs exceed the electronic Zeeman energy, as is approximately true for both Fe(III)-TSPP and Mn(III)-TSPP over the range of laboratory field strengths in MRD experiments].

In summary, our prior investigations of the three metalloporphyrins, Cr(III)-TSPP (Ref. 3) ($S=3/2$), Mn(III)-TSPP (Refs. 1 and 2) ($S=2$), and Mn(II)-TSPP (Ref. 4) ($S=5/2$)

a)Electronic mail: rrsharp@umich.edu

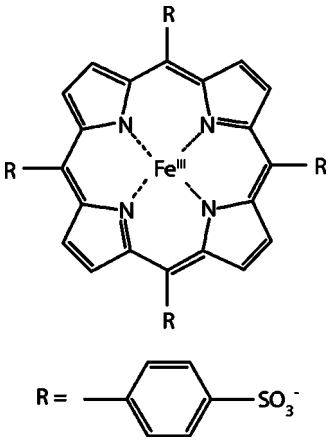

FIG. 1. Structure of Fe^{III}-TSPP.

(the latter using the data from Bryant *et al.*[5]), have found qualitative differences in the relaxation mechanisms arising from characteristic differences in the spin physics. The present study extends the series with Fe(III)-TSPP, a model $S=5/2$ spin system. This system differs from Mn(II)-TSPP (also $S=5/2$) in that the zfs is much larger, a fact that has critical consequences for the relaxation mechanism.

We have also investigated the effect of a large permanent zfs, as occurs in Fe(III)-TSPP, on the magnetic-field dependence of electron-spin relaxation. Calculations which include effects of the static zfs interaction indicate that the electron spins T_1 and T_2 are nearly field independent across the range of the MRD experiment, in agreement with experiment but in marked disagreement with Bloembergen–Morgan theory.[6]

II. EXPERIMENT

Fe(III)-TSPP, purchased from Frontier Scientific (Logan, Utah), was used as supplied. Aqueous buffered samples, containing 1.0–1.2-mM Fe(III)-TSPP and 50.0-mM total buffer, were prepared with integer pH values in the range pH 1–5. Hydrion dry buffer salts from Aldrich were used: pH 2 and 3 were biphthalate/sulphamic acid, pH 4 was biphthalate, and pH 5 was phosphate; the pH 1 buffer was certified standard (HCl/NaCl) from Fisher Scientific. Distilled, de-ionized water was taken from a Barnsted millipore filtration system with both ionic and organic sections. The samples were placed in 7-mm, acid-washed borosilicate test tubes, degassed by a series of five freeze-pump-thaw cycles, and sealed under vacuum. UV-visible absorption spectra were collected on a Shimadzu UV1601 spectrometer. NMR T_1 relaxation times were measured at frequencies of 0.6–70 MHz at 20 °C using a custom-built tunable NMR spectrometer.[2]

III. THEORY

The magnetic-field dependence of the NMR-PRE is a consequence of the electron-spin dynamics, which is in turn driven by the electron-spin Hamiltonian. This section describes the electron-spin Hamiltonian, the spin level diagram, and the spin wave functions for $S=5/2$ in the vicinity of the zfs limit. We then describe the influence of specific quadratic and fourth-order zfs tensor components on the electron-spin dynamics and the NMR-PRE.

A. Electron-spin Hamiltonian for $S=5/2$

The electron-spin Hamiltonian is assumed to be comprised of Zeeman and zfs terms,

$$H_S(\beta,\gamma;t) = H_{\mathrm{Zeem}} + H^{\circ}_{\mathrm{zfs}}(\beta,\gamma;t), \tag{1a}$$

$$= g_e\beta_e\vec{\boldsymbol{B}}_0\vec{\boldsymbol{S}} + \sum B^q_k\hat{O}^q_k. \tag{1b}$$

The Hamiltonian, $H^{\circ}_{\mathrm{zfs}}(\beta,\gamma;t)$, of the permanent zfs interaction depends on the polar angles (β,γ), specifying the orientation of the laboratory magnetic field in the zfs principal-axis system (PAS). In the presence of Brownian reorientation, it is also a stochastic function of time. The sum on the right-hand side (rhs) of Eq. (1b) includes energy terms which are of even order in the electron-spin operators. These are commonly (though somewhat ambiguously[7]) called zfs interactions, and we use the term as well. The quantities, B^q_k, are numerical coefficients, and the factors, O^q_k, are operator equivalents, the functional forms of which are listed for $k \leqslant 4$ in the Appendix. In Eq. (1b), the zfs terms are expressed in the molecule-fixed PAS of the zfs tensor [this coordinate system denoted by the superscripting karat ($\wedge$) on the spin operators]. When expressed in the PAS, the only nonvanishing zfs components are those with q and k even (a result of the even parity of the zfs interaction), $k \leqslant 4$ (required for $S=5/2$ by the dimensionality of the spin space), and $q \leqslant k$. Thus the general zfs Hamiltonian for $S=5/2$ is

$$H^{\circ}_{\mathrm{zfs}} = B^0_2\hat{O}^0_2 + B^2_2\hat{O}^2_2 + B^0_4\hat{O}^0_4 + B^2_4\hat{O}^2_4 + B^4_4\hat{O}^4_4. \tag{2}$$

In the ESR literature, the quadratic zfs parameters D and E (in cm^{-1}) are often used instead of B^0_2 and B^2_2, the conversions being $D=3\tilde{B}^0_2$ and $E=\tilde{B}^2_2$, where $\tilde{B}^q_k = B^q_k(10^2hc)^{-1}$ has units of wave numbers. Planck's constant, h, and the speed of light, c, are in Système International (SI). Equation (2) is written in compact form following Abragam and Bleaney[8] rather than in expanded form (see Rudowicz[9]), which has been used by Fries and co-workers[10–13] in their recent studies of Gd(III) complexes.

The form of Eq. (2) is further constrained by the rotational symmetry of the crystal-field potential, V. The zfs terms in Eq. (1b) arise from the components of V which vary upon rotation about the principal axis as $\cos(q\phi)$. Cylindrical, orthorhombic, and tetragonal zfs terms ($q=0$, 2, and 4, respectively) arise from the parts of V that transform on rotation as $\cos(0\phi)$, $\cos(2\phi)$, and $\cos(4\phi)$, respectively. In Fe(III)-TSPP, Fe(III) lies on a fourfold rotation axis, and the orthorhombic terms ($q=2$) vanish. Thus, H°_{zfs} has two cylindrical terms and one tetragonal term,

$$H^{\circ}_{\mathrm{zfs}} = B^0_2\hat{O}^0_2 + B^0_4\hat{O}^0_4 + B^4_4\hat{O}^4_4. \tag{3}$$

The electron-spin level diagram and spin eigenfunctions for $S=5/2$ in the vicinity of the zfs limit are shown in Fig. 2. Frames a–c show the effect of turning on successive terms of Eq. (3), and frame (d) shows the effect of adding a small Zeeman interaction. In the cylindrical zfs limit [Figs. 2(a) and 2(b)], the spin eigenfuctions can be taken as the circularly polarized functions, $|\pm 1/2\rangle$, $|\pm 3/2\rangle$, and $|\pm 5/2\rangle$, spatially quantized along the unique axis, $\hat{z}$, of the zfs tensor.

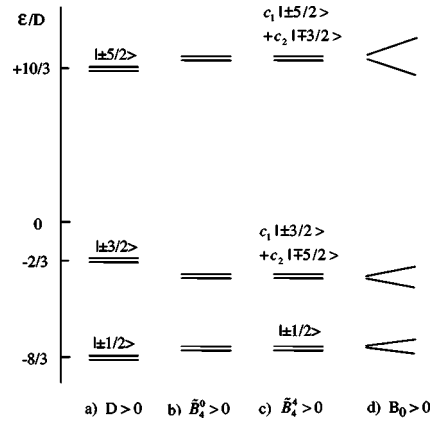

FIG. 2. Energy levels and eigenfunctions for an electron spin $S=5/2$ in the vicinity of the zfs limit. Frames a–c show the effect of adding successive zfs terms in Eq. (3) of the text. Frame d shows the effect of adding a small Zeeman field, B_0. Energies are in units of the zfs parameter, D.

When only the cylindrical quadratic zfs term, $\tilde{B}_2^0\hat{O}_2^0$ (where $D=3\tilde{B}_2^0$) is present, the energy levels comprise three Kramers doublets, $m_S=\pm 1/2$, $\pm 3/2$, and $\pm 5/2$, with adjacent levels separated by 2D and 4D. Figure 2(b) shows the additional effect of the fourth-order cylindrical zfs term, $\tilde{B}_4^0\hat{O}_4^0$. This term alters the energies of the doublets in the first-order perturbation theory (taking the zero-order Hamiltonian to be $H_{\mathrm{zfs}}^{*}=B_2^0\hat{O}_2^0$), but it does not mix the circular zfs-limit eigenfunctions, since $[\hat{O}_2^0,\hat{O}_4^0]=0$. Figure 2(c) shows the effect of the fourth-order tetragonal term, $B_4^4\hat{O}_4^4$. This term is off diagonal in the eigenbasis of $\hat{O}_2^0$ and thus does not affect the energies in the first order. From the Appendix, the operator equivalent can be written as $\hat{O}_4^4=(1/2)(\hat{S}_+^4-\hat{S}_-^4)$, which mixes the eigenfunctions of $\hat{O}_2^0$ for which $\Delta m_S=\pm 4$. The first-order eigenfunctions are

$$|\pm 3/2\rangle' \Rightarrow c_1|\pm 3/2\rangle + c_2|\mp 5/2\rangle, \tag{4a}$$

$$|\pm 5/2\rangle' \Rightarrow c_1|\pm 5/2\rangle + c_2|\mp 3/2\rangle, \tag{4b}$$

$$|\pm 1/2\rangle' \Rightarrow |\pm 1/2\rangle. \tag{4c}$$

The mixing ratio, (c_2/c_1), is plotted as a function of the ratio of zfs parameters, $\tilde{B}_4^4/D$ in Fig. 3. The effects of $\tilde{B}_4^4$-induced wave-function mixing are the primary concern of our study. This mixing generates nonzero off-diagonal matrix elements of $\langle\hat{S}_x\rangle$ and $\langle\hat{S}_y\rangle$ within the $m_S=\pm 3/2$ and $m_S=\pm 5/2$ Kramers doublets, giving rise to a large Zeeman dispersion, which is the principal feature of the experimental MRD profile.

The addition of a Zeeman term to the zfs Hamiltonian of Eq. (3) splits the non-Kramers doublets [Fig. 2(d)] by an amount that depends on the orientation of the unique axis of the zfs tensor and $\vec{\boldsymbol{B}}_0$. The spread of the energy levels in a powder sample is shown in Fig. 4. The range of Zeeman field strengths in the MRD experiments discussed below is restricted to the low-field ($B_0<2$ *T*) portion of the diagram.

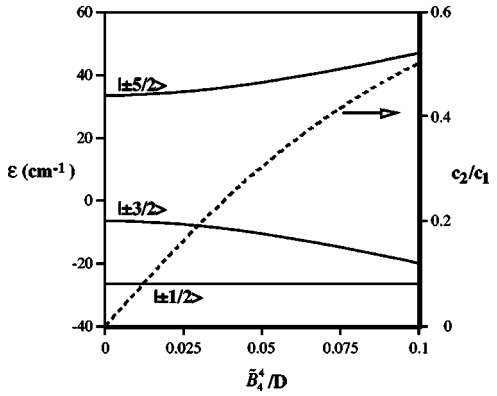

FIG. 3. ZFS-limit energies and spin eigenfunctions of $S=5/2$ as a function of the fourth-order zfs coefficient, $\tilde{B}_4^4$, in units of D. The calculations assumed $D=10$ cm^{-1}, $E=0$, $\tilde{B}_4^0=0$, and $B_0=0$. The dashed curve gives the mixing coefficients defined in Eqs. (4).

B. NMR paramagnetic relaxation enhancement (PRE)

The NMR-PRE of water protons due to a dissolved paramagnetic ion can be written as

$$R_1 = R_{1p} + R_{1,\mathrm{os}} + R_{1,\mathrm{dia}}, \tag{5}$$

where the terms on the rhs arise, respectively, from the relaxation of protons in the first coordination sphere of the metal, relaxation due to uncoordinated water protons (the outer sphere or translational contribution), and the diamagnetic background. R_1 is assumed to result only from the magnetic dipole–dipole couplings, since the scalar contribution to the water proton R_1 is very small.

Inner sphere relaxation of the water resonance (R_{1p}) results from the chemical exchange of water protons between the first coordination sphere of the metal ion to the unbound solvent pool. This contribution is given by[14]

$$R_{1p} = f_M/(T_{1M} + \tau_M), \tag{6}$$

where f_M is the mole fraction of exchangeable solvent protons in the bound site, T_{1M} is the relaxation time of bound protons, and τ_M is the chemical exchange residence time. The Zeeman-limit Solomon–Bloembergen–Morgan (SBM) theory of R_{1p} is well known.[6,15,16] For Fe(III)-TSPP, the static zfs is large, and theory is needed which includes the effects of $H_{\mathrm{zfs}}^{\circ}(\beta,\gamma;t)$. The influence of a permanent cylindrical zfs tensor on the relaxation mechanism of $S=3/2$ and $S=5/2$ complexes was first described quantitatively in the

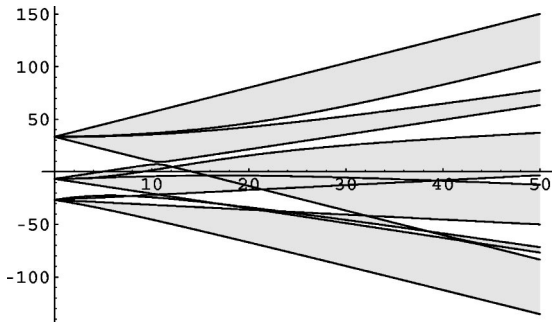

FIG. 4. The spread of energy levels for $S=5/2$ in a powder with $D=10$ cm^{-1}.

1980s by Bertini and co-workers[17,18] in Florence and by the Swedish group of Benetis and co-workers.[19–22] The latter have developed a very general formulation of the problem based on the stochastic Liouville equation (SLE). This approach has been used to model the stochastic motions of the zfs tensor that are responsible for electron-spin relaxation[23–27] as well as to provide model calculations characterizing the NMR-PRE phenomenon in motional regimes where Redfield theory is not valid.[28–32]

The present study uses theory that has been developed at the University of Michigan over the past 15 years[1,33–39] and implemented in the computer program PARELAX2,[3,4,37,40] an evolved form of our earlier program PARELAX.[41] The theory incorporates a spin Hamiltonian of the form of Eq. (1b) and describes the effects of Brownian reorientation at various levels of approximation, of which two—spin dynamics (SD) simulation and the constant H_S approximation—are employed in the present study. The theory implemented in PARELAX2 is described in Ref. 42. The crux of the theoretical problem lies in calculating the time correlation function (tcf) of the electron-nuclear dipole–dipole Hamiltonian, $\{\langle H_{IS}(t)H_{IS}(0)\rangle\}_{ea}$, in circumstances where $H_S(\beta,\gamma;t)$ in Eq. (1) is a stochastic function of time due to Brownian reorientation. The angular brackets denote a trace over spin variables, and the braces denote an ensemble average over molecular degrees of freedom. In the presence of Brownian reorientation, the electron-spin eigenfunctions and eigenfrequencies are also stochastic functions of time. In addition to modulating $H_S(\beta,\gamma;t)$, reorientation also modulates the interspin vector, $\vec{r}_{IS}(t)$, damping the dipole–dipole tcf. Furthermore the motions of $\vec{r}_{IS}(t)$ and $H_S(\beta,\gamma;t)$ are correlated.

1. Spin dynamics (SD) simulation

SD calculates the dipole–dipole tcf of the electron-nuclear dipole–dipole Hamiltonian in a very direct way as a thermal ensemble of trajectories in the time domain. Molecular reorientation is modeled classically using the random walk model of Ivanov,[43] and the motion of the electron-spin operators is propagated quantum mechanically. The algorithms have been described.[2,4,37,40,44] While much less detailed than a full molecular-dynamics (MD) simulation (see Odelius *et al.*[45,46]), SD provides a realistic and efficient description of the motional aspects of the problem for rigid molecules, and the algorithms readily accommodate a spin Hamiltonian of any form. A limitation is that multiexponential electron-spin relaxation cannot readily be incorporated into the time-domain calculation.

Our SD methods are similar in approach to the Monte Carlo (MC) formulation used by Fries *et al.*[47] to simulate ESR line shapes. Both of these time-domain calculations differ greatly from SLE, in which the tcf's of the coupled nuclear- and electron-spin systems are computed as the solution of a stochastic Liouville equation of the coupled spin and molecular degrees of freedom. However, the three approaches (SD, MC, and SLE) attack the core problem of describing the Brownian motion of $H_S(t)$ at a similar level of approximation. They differ substantially in their treatment of electron-spin relaxation.

2. Constant H_S theory

A deficiency of SD is that time-domain simulations do not readily incorporate level-specific electron-spin relaxation (i.e., for $S=5/2$, electron spin-relaxation times which differ in the $m_S=\pm 1/2$, $\pm 3/2$, and $\pm 5/2$ Kramers doublets). Also, SD simulations lack physical transparency in terms of the contributions of specific eigenstates, spin matrix elements, etc. These deficiencies are remedied in part in the constant H_S approximation, which treats the electron-spin Hamiltonian as in a powder; i.e., the reorientational time dependence of $H^{\circ}_{\mathrm{zfs}}(\beta,\gamma;t)$ in Eq. (1a) is neglected. Thus $H_S(\beta,\gamma;t)$ can be written as $H_S(\beta,\gamma)$. Although the effect of Brownian reorientation on $H_S(\beta,\gamma;t)$ is neglected, the stochastic motions of $\vec{r}_{IS}(t)$, which damp the dipole–dipole tcf, are retained in the form of a damping factor, $\exp(-t/\tau_R)$.

In the constant H_S algorithms of PARELAX2, $H_S(\beta,\gamma)$ is diagonalized at a sequence of discrete molecular orientations, at each of which the NMR relaxation rate, R_{1M}, is calculated as a sum of contributions due to spin matrix elements, $\langle\mu|\hat{S}^{(1)}_p|\nu\rangle$, evaluated in the eigenbasis of $H_S(\beta,\gamma)$. These contributions are averaged spatially using a model in which (β,γ) are defined by the set of 92 orientations corresponding to the vertices and face centers of the truncated icosahedron (buckeyball). In the constant H_S expressions, the contributions to R_{1M} of specific spin matrix elements are isolated in a way that is not possible in the time-domain simulations of SD, because in SD the eigenbasis is time dependent. The constant H_S formulation also incorporates multiexponential electron-spin relaxation times, which SD does not. Neither SD simulation nor constant H_S provides an entirely satisfactory description; the former provides a more realistic description of the effects of Brownian motion, the latter provides a transparent physical picture and is able to incorporate multiexponential electron-spin relaxation times. We use the two methods in parallel to provide as full a picture of the relaxation mechanism as possible.

The molecular-frame (MF) constant H_S expression for R_{1M} is[42]

$$R_{1M} = -48\pi\left(\frac{\gamma_I g_e \beta_e}{r_{IS}^3}\right)^2\left(\frac{\mu_o}{4\pi}\right)^2 \sum_{q,q'=-1}^{1}\sum_{p,p'=-1}^{1} \times\begin{bmatrix}1 & 2 & 1\\ p & (q-p) & -q\end{bmatrix}\begin{bmatrix}1 & 2 & 1\\ p' & (q'-p') & -q'\end{bmatrix} \times(-1)^{q+q'}Y_{2,q-p}(\hat{\theta},\hat{\varphi})Y_{2,q'-p'}(\hat{\theta},\hat{\varphi}) \times\left\{\mathcal{D}^{(1)}_{q,+1}(\alpha,\beta,\gamma)\mathcal{D}^{(1)}_{q',-1}(\alpha,\beta,\gamma) \times(2S+1)^{-1}\sum_{\mu,\nu}\langle\mu|\hat{S}^{(1)}_p|\nu\rangle\langle\nu|\hat{S}^{(1)}_{p'}|\mu\rangle\hat{j}_p(\omega_{\mu\nu})\right\}_{ea} \quad (7a)$$

$$\hat{j}_p(\omega_{\mu\nu}) = \frac{\hat{\tau}^{(\mu)}_{d,p}}{1+(\omega_I-\omega_{\mu\nu})^2(\hat{\tau}^{(\mu)}_{d,p})^2}. \quad (7b)$$

The quantities in square brackets are 3-j symbols, r_{IS} is the interspin distance, and μ_0 is permeability of space. The second-rank spherical harmonics, $Y_{2,q}(\hat{\theta},\hat{\varphi})$, have as argu-

ments the polar angles of the interspin vector, $\vec{r}_{IS}$ with respect to the zfs unique axis, $\hat{z}$. The braces denote an average over molecular orientations, which is computed within PARELAX2 using the buckeyball model described above, neglecting the Brownian motion of $H_S(\beta,\gamma)$. The spin matrix elements and eigenfrequencies, $\omega_{\mu\nu}$, depend on molecular orientation, but the dipolar correlation times, $\hat{\tau}_{d,r}$, do not (see below). The orientation of the laboratory field, $\vec{\boldsymbol{B}}_0$, in the MF is specified by the Euler angles (α,β,γ). The Wigner rotation matrix elements, $\mathcal{D}^{(1)}_{q,\pm 1-p}(\alpha,\beta,\gamma)$, transform first-rank spherical tensor operators from the laboratory frame (LF) to the MF.

The dipolar correlation time in Eq. (7b) is defined as

$$(\hat{\tau}_{d,r})^{-1} = (\tau_R)^{-1} + (\hat{\tau}_{S,r})^{-1} + (\tau_M)^{-1}. \tag{8}$$

The second term on the r.h.s. is the electron spin relaxation rate defined in the MF. Eq. (8) assumes that electron spin decay is averaged over eigenstates.[51] The quantity, τ_M, in the third term is the correlation time for chemical exchange of solvent protons.

The constant H_S algorithms of PARELAX2 [e.g., Eqs. (7) and (8)] are based on the theoretical development of Ref. 38 and are described more fully in Ref. 42. These algorithms differ from those of our earlier program PARELAX,[41] the approach of which is similar to that described by Bertini *et al.*[48] Within SLE, "decomposition[49] (DC)" represents a similar level of approximation.

C. Electron-spin relaxation

The electron-spin relaxation times, $\hat{\tau}_{S,r}$, in Eq. (4) in general depend on the eigenstate (μ) and the spatial polarization $(r=\hat{x},\hat{z})$,[50] and in this general case are written as $\hat{\tau}^{(\mu)}_{S,r}$. Usually we lack sufficient physical information to calculate meaningful eigenstate-specific relaxation times, and use instead the eigenstate-averaged quantities, $\hat{\tau}_{S,r}$, of Ref. 51. These parameters describe the collisional zfs relaxation mechanism (see below) and describe spin decay along MF, rather than along LF, axes.

The mechanism of electron-spin relaxation for $S \geqslant 1$ metal ions involves thermal modulation of the zfs tensor due to (1) Brownian reorientation of the zfs principal axes, (2) collisional modulation of the zfs tensor components, and (3) zfs modulation due to vibrational damping.[52] The reorientational mechanism is described quantitatively in a SD simulation, requiring only the permanent zfs parameters and $\tau^{(2)}_R$ as input (SLE and MC have similar capabilities). Relaxation due to vibrational damping has been ignored in most (but not all[25,53]) previous studies, and we do likewise.

The collisional zfs mechanism is described in the Zeeman limit by the well-known theory of Bloembergen and Morgan[6] (BM). For Fe(III)-TSPP, theory is needed which includes the effect of $H^{\circ}_{\mathrm{zfs}}(\beta,\gamma;t)$. Westlund[54] has derived zfs-limit Redfield expressions for $S=1$ that are analogous to those of BM theory. These expressions have been generalized to non-Redfield situations $(\tau_v \geqslant \tau_S)$ by Bertini *et al.*[55] Subsequently, Sharp and Lohr[50] derived Redfield expressions that are valid for arbitrary electron spin at all field strengths, i.e., for the zfs and Zeeman limits as well as for the intermediate regime ($H^{\circ}_{\mathrm{zfs}} \approx H_{\mathrm{Zeem}}$). Sharp[51] later simplified these results to provide the following approximate eigenstate-averaged expressions for $\hat{\tau}_{S,r}$ $(r=z,x)$:

$$(\hat{\tau}_{S,r})^{-1} = c_r \sum_{q=1}^{5} n_q^{(r)} \left\{ \sum_{\mu,\nu} |\langle\mu|\hat{S}^{(2)}_q|\nu\rangle|^2 j(\omega_{\mu\nu}) + c.t. \right\}_{ea}, \tag{9a}$$

$$c.t. = 3^{1/2} c_r \sum_{\mu,\nu} \langle\mu|\hat{S}^{(2)}_1|\nu\rangle\langle\nu|\hat{S}^{(2)}_2|\mu\rangle [2j(\omega_{\mu\nu})], \tag{9b}$$

$$c_r = 3[S(S+1)(2S+1)]^{-1}(\Delta_t^2/5), \tag{9c}$$

$$j(\omega) = \tau_\nu/(1+\omega^2\tau_\nu^2). \tag{9d}$$

The relaxation times depend on two physical parameters, namely, Δ_t^2, the mean-square value of the transient zfs tensor associated with collisional distortion, and τ_ν, the correlation time for distortion. The quantities, $\hat{S}^{(2)}_q$, are second-rank cartesian tensor functions of the spin operators,[51] and the quantities, $n_q^{(r)}$, are integer coefficients which occur in double commutators of the spin operators.[51] The matrix elements are evaluated in the eigenbasis of $H_S(\beta,\gamma)$. In the intermediate regime of field strengths, Eqs. (9a) and (9b) need to be averaged over molecular orientations with respect to B_0. This is carried out in PARELAX2 using the "buckeyball" algorithm described above.

Further information concerning the relaxation times of Eqs. (9) is in Refs. 3, 44, and 51. Equations (6) are Redfield expressions which assume that zfs distortion is fast compared to electron-spin relaxation $(\tau_v < \tau_S)$, a condition that we expect to be valid Fe(III)-TSPP, for which $\tau_{S1} \approx 100$ ps at room temperature.[56] Methods have been developed which relax the assumption of fast distortional motions $(\tau_v < \tau_S)$,[57] but these are not needed for this analysis.

IV. THEORETICAL SIMULATIONS

Figures 5–9 show the results of constant H_S calculations illustrating the influence of cylindrical (second and fourth order), tetragonal (fourth order), and orthorhombic (second order) zfs tensor components on the R_1 MRD profile for $S=5/2$. Figure 10 illustrates the effect of a permanent zfs interaction on the magnetic-field dependence of electron-spin relaxation for $S=5/2$. The interpretation of the MRD profile for $S=5/2$ when H°_{zfs} contains only quadratic zfs terms has been discussed previously by Westlund *et al.*,[22] Banci *et al.*,[17] Miller and Sharp,[4] and Sharp.[58] The influence of zfs orthorhombicity for $S=5/2$ has been discussed by Nilsson and Kowalewski.[30] Some of these results will be recapitulated in order to provide a unified interpretation of the relaxation mechanism.

A. The cylindrical zfs limit

Figure 5 shows the effect of an increasing cylindrical zfs term, $D(=3\tilde{B}^0_2)$, on the MRD profile for $S=5/2$ with other zfs tensor elements set to zero. The calculations assume that electron-spin relaxation is magnetic-field independent, and that the water proton lies at a near-axial location in the MF ($\theta_{IS}=0.30$ rad). The arrows indicate the direction of increas-

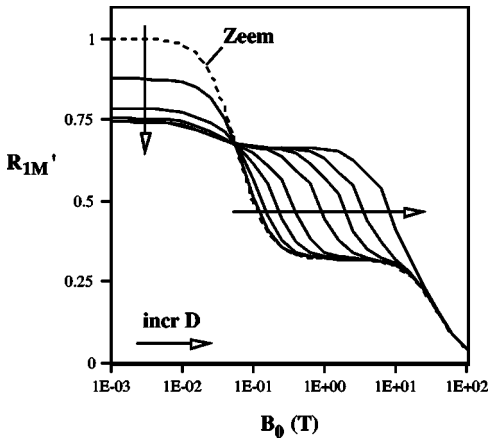

FIG. 5. Effect of the cylindrical quadratic zfs parameter $D(=\tilde{B}_2^0/3)$ on the MRD profiles for $S=5/2$. The constant H_S calculations are normalized to the low-field, Zeeman-limit R_{1M} value. D increases through the values, $D=0$ (dashed), 0.02, 0.05, 0.10, 0.20, 0.5, 1.0, 2.0, and 5.0 cm^{-1}. Other parameters were $\tau_{dip,r}=100$ ps (fixed) and $\theta_{IS}=0.28$ rad.

ing D, varying from an initial value of $D=0$ (the Zeeman limit) to a final value of $D=5$ cm^{-1}. Based on prior measurements of D for ferric porphyrins (see below), we expect $D \geqslant 5$ cm^{-1} for Fe(III)-TSPP, i.e., that D for Fe(III)-TSPP is larger than the maximum value plotted in Fig. 5.

The Zeeman-limit profile (dashed) exhibits two well-defined dispersions, one centered at the low field where $(\omega_S \pm \omega_I)\tau_{d,\perp}=1$, the other at the high field where $\omega_I \tau_{d,z}=1$. When $D \neq 0$, the profile exhibits as many as three dispersive features. Interestingly, there is an intermediate field strength at which the NMR-PRE is invariant to changes in D (reminiscent of an isosbestic point in UV-vis spectra). Banci *et al.*[17] found that this effect occurs for $\theta_{IS}=0°$ but not for 90°.

1. The low-field dispersive feature

The dispersion centered at the lowest field has a physical origin like that in the Zeeman-limit profile, i.e., it results from the Zeeman splitting of electron-spin levels. In the presence of a permanent zfs interaction of strength, $D \geqslant 0.01$ cm^{-1}, this dispersion decreases in amplitude, approaching a constant small amplitude when $D \geqslant 0.01$ cm^{-1}. In terms of constant H_S theory [Eq. (7)], the low-field dispersion arises from the off-diagonal transverse spin matrix elements, $\langle \mp 1/2|\hat{S}_{x,y}|\pm 1/2\rangle$, which couple the levels of the $m_S=\pm 1/2$ Kramers doublet. In the cylindrical zfs limit, these are the only off-diagonal matrix elements that contribute significantly to the NMR-PRE; the other nonvanishing one-quantum (1Q) matrix elements (e.g., $\langle \pm 1/2|\hat{S}_{x,y}|\pm 3/2\rangle$) oscillate with large eigenfrequencies, suppressing the associated spectral density functions in Eq. (7). In the Zeeman-limit profile (dashed), the low-field dispersive feature is much larger than in the zfs limit due to the fact that all of the off-diagonal 1Q matrix elements of $\langle \hat{S}_x \rangle$ and $\langle \hat{S}_y \rangle$ contribute to the relaxation efficiency.

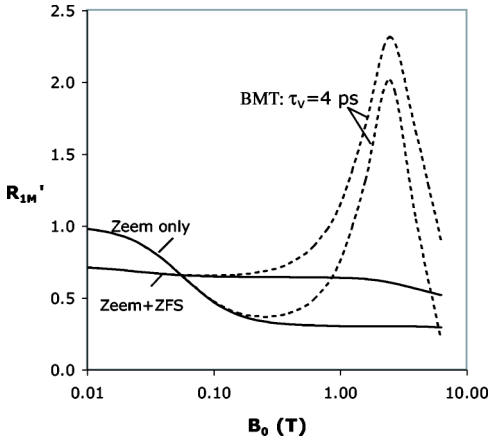

FIG. 6. Effect of magnetic-field-dependent electron-spin relaxation on the MRD profile. The solid lines assume that electron-spin relaxation is magnetic-field independent (fixed $\tau_{d,r}=100$ ps, $\theta_{IS}=0.3$ rad) and (1) that zfs interactions are zero (Zeem only) or (2) that a cylindrical zfs tensor with $D=5$ cm^{-1} is present (Zeem+zfs). The dashed curves assume, in addition, that $\tau_S(=\tau_{d,r})$ is given by BM theory with $\tau_v=4$ ps. The calculations are normalized to the low-field, Zeeman-only limit.

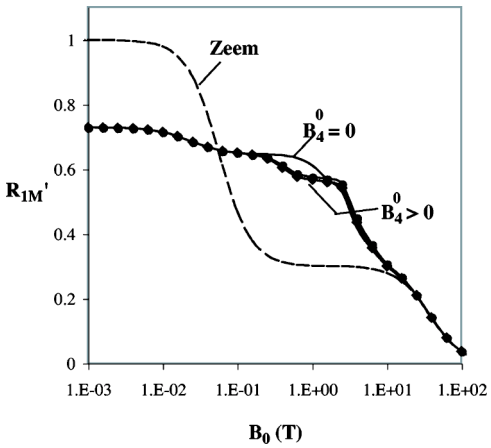

FIG. 7. Effect of the cylindrical fourth-order zfs term, $\tilde{B}_4^0$, on the R_{1M} MRD profiles for $S=5/2$. The calculations are like those in Fig. 5 except that $D=3$ cm^{-1} and $\tilde{B}_4^0/D=0$ (no symbol), 0.05 (diamonds), or 0.1 (circles).

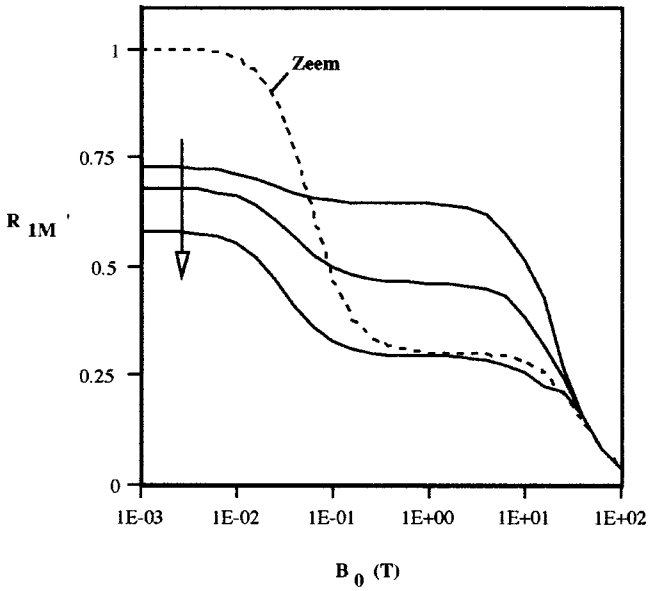

FIG. 8. Effect of the tetragonal fourth-order zfs term, $\tilde{B}_4^4$, on the R_{1M} MRD profiles for $S=5/2$. The calculations are like those in Fig. 5 except that $D \approx 10$ cm^{-1} and $\tilde{B}_4^4/D=0$, 0.05, or 0.1, increasing with the arrow.

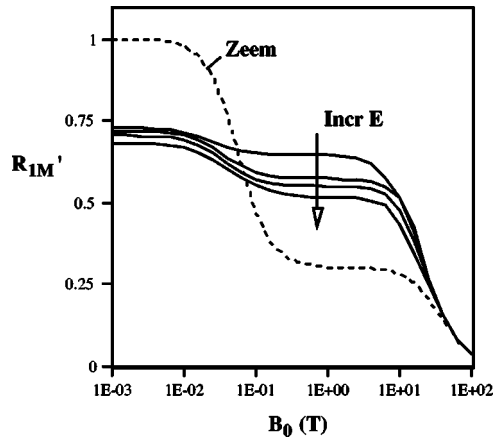

FIG. 9. Effect of the orthorhombic quadratic zfs term, $E=\tilde{B}_2^2$, on the R_{1M} MRD profiles for $S=5/2$. The calculations are like those in Fig. 5 except that $D=10$ cm^{-1} and $E/D=0$, 0.1, 0.2, or 0.3 (increasing with the arrow).

2. The midfield dispersive feature

When the permanent zfs is substantial ($D \geqslant 0.1$ cm^{-1} in Fig. 5), essentially all of the relaxation efficiency other than that associated with the small low-field dispersive feature results from diagonal spin matrix elements of $\langle \hat{S}_z \rangle$. These matrix elements have zero frequency ($\omega_{\mu\mu}=0$) and do not produce Zeeman-type dispersions. Rather, the midfield dispersion arises from the change of spatial quantization of the spin motion which occurs when the spin system passes between the zfs and Zeeman limits. The midfield position of the dispersive feature is located approximately where $\omega_S \approx 2\omega_D$ (ω_S is the electron Larmor frequency and $\omega_D = 2\pi cD$). The form of this feature depends strongly upon θ_{IS},[17,30,58] falling with increasing B_0 for an axial nuclear location and rising with increasing B_0 for an equatorial location (Fig. 5 assumes a near-axial location).

3. The high-field dispersion

The high-field dispersion centered near 30 T occurs where $\omega_I \tau_{d,x}=1$ This feature, which is usually not observed in the range of field variation of MRD experiments, occurs when the nuclear Larmor frequency is displaced outside the dipolar power band of the electron-spin time correlation function.[39]

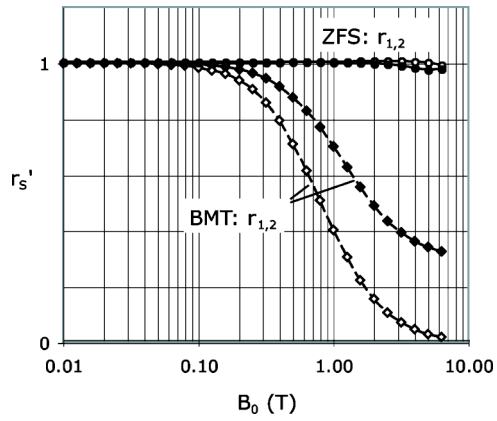

FIG. 10. Calculated electron-spin relaxation rates as a function of magnetic-field strength for $S=5/2$. Calculations were based on BM theory (BMT: dashed lines and diamonds) or Eqs. (10) (zfs: solid lines and circles). All calculations assumed $\tau_v=4$ ps. The zfs calculations assumed $D=10$ cm^{-1} and $\tilde{B}_4^4/D=0.1$. Relaxation rates (r_1) along z are the unfilled symbols; those along x are the filled symbols.

4. Magnetic-field dependence of electron-spin relaxation

Figure 6 illustrates the effect on the MRD profile of magnetic-field dependence in the electron-spin relaxation time. Profiles are shown for the Zeeman limit ($D=0$) and for the vicinity of the cylindrical zfs limit ($D=10$ cm^{-1}). The dashed curves were calculated assuming $\tau_d=\tau_S$, with τ_S calculated by BM theory and $\tau_v=4$ ps. Calculations assuming a field-independent τ_S (solid lines) are also shown. Magnetic-field dependence in τ_S produces a large dispersive feature in the high-field region of the profile. This feature, which is commonly been observed in the MRD profiles for Mn(II) when $\tau_R^{(2)}$ is long, is not observed in the experimental profiles for Fe(III)-TSPP (see below).

The reason for the evident lack of field dependence in τ_S in the experimental profiles was investigated in the calculations of Fig. 10, which illustrate the effect of a large permanent zfs ($D=10$ cm^{-1}) on τ_{S1} and τ_{S2}. Calculations based on both BM theory and on Eqs. (9) are shown. Both sets of calculations assumed $\tau_v=4$ ps and are normalized to the $B_0=0$ calculation. Clearly, a large zfs suppresses the magnetic-field-dependent spectral density functions in Eqs. (9), resulting in field independence in $\tau_{S1,2}$.

B. The fourth-order cylindrical zfs term, $\tilde{B}_4^0$

The influence of $\tilde{B}_4^0$ on the constant H_S profile is very small, as shown in Fig. 7. This term influences the separations of the non-Kramers doublets (Fig. 2), but it does not mix the eigenfunctions of the zero-order zfs-limit Hamiltonian ($H_{\text{zfs}}^{\circ}=B_2^0\hat{O}_2^0$). As described above, the off-diagonal matrix elements of Eq. (7) contribute very little to the NMR-PRE, and thus the influence of $\tilde{B}_4^0$ on the interdoublet level spacings is unimportant for the NMR-PRE. Although $\tilde{B}_4^0$ does not affect the spin eigenfunctions in the zfs limit, it has a small effect on the eigenfunctions when $B_0>0$, thus producing minor perturbations of the MRD profiles, as shown in Fig. 7.

C. The fourth-order tetragonal zfs term, $\tilde{B}_4^4$

Figure 8 shows the dependence of the MRD profile on the presence of a tetragonal fourth-order zfs component, $\tilde{B}_4^4$ (increasing with the arrow). As the ratio $\tilde{B}_4^4/D$ increases, the magnitude of the low-field Zeeman-type dispersion increases dramatically, becoming qualitatively much more like a Zeeman-limit profile in appearance. This phenomenon results from the $\tilde{B}_4^4$-induced wave-function mixing illustrated in Fig. 3. As described above, the tetragonal fourth-order zfs term mixes circular basis functions with $\Delta m_S=\pm 4$, thus mixing $|\pm 3/2\rangle$ with $|\mp 5/2\rangle$ [Eqs. (4)]. As a consequence, the 1Q transverse spin matrix elements connecting these basis

states are allowed, giving rise to the following nonzero terms in the summation of Eq. (7):

$$T_{5/2}^{(4)} = c_1 c_2 |\langle \pm 3/2 | \hat{S}_{x(y)} | \pm 5/2 \rangle|^2 \frac{\hat{\tau}_{S,x(y)}^{(5/2)}}{1 + [\Delta\omega_{5/2} \hat{\tau}_{S,x(y)}^{(5/2)}]^2}, \quad (10a)$$

$$T_{3/2}^{(4)} = c_1 c_2 |\langle \pm 5/2 | \hat{S}_{x(y)} | \pm 3/2 \rangle|^2 \frac{\hat{\tau}_{S,x(y)}^{(3/2)}}{1 + [\Delta\omega_{3/2} \hat{\tau}_{S,x(y)}^{(3/2)}]^2}. \quad (10b)$$

The transition frequencies, $\Delta\omega_{3/2}$ and $\Delta\omega_{5/2}$, are the intradoublet Zeeman splittings of the $m_S = \pm 3/2$ and $\pm 5/2$ Kramers manifolds. These terms are suppressed with increasing B_0, giving rise to a Zeeman-type dispersion. The amplitude of this dispersion depends on the mixing ratio, $\tilde{B}_4^4/D$, rather than on the absolute magnitude of $\tilde{B}_4^4$.

D. The orthorhombic zfs term, *E*

Fe(III)-TSPP lacks orthorhombic zfs terms due to its four-fold rotation symmetry, but it is of interest to consider the effect of these terms in cases where they are present. Figure 9 shows the dependence of the zfs-limit MRD profile on the zfs parameter $E(=\tilde{B}_2^0)$ in the range $0 \leqslant E \leqslant 0.3$ (increasing with the arrow). The calculations assumed $D = 10\ \mathrm{cm}^{-1}$ and $\tilde{B}_4^4 = 0$. The effect of E on the profile is qualitatively similar to, but smaller than that of the $\tilde{B}_4^4$ term, i.e., the amplitude of the low-field dispersion near $\omega_S \hat{\tau}_{d,z} = 1$ increases by an amount which depends on the ratio, E/D. Orthorhombicity mixes zfs-limit basis functions with $\Delta m_S = \pm 2$, thus introducing $\langle \pm 3/2 | \hat{S}_{x,y} | \mp 1/2 \rangle$ character into the $m_S = \pm 3/2$ spin manifold. The contribution of these matrix elements to R_{1M}, while significant, is smaller than that produced by $\tilde{B}_4^4$.

V. THE MRD PROFILE OF Fe(III)-TSPP

Fe(III)-TSPP provides an interesting experimental example of the near zfs-limit situation for $S = 5/2$, with H_{zfs}° given by Eq. (3). D has not been measured for bisaqua Fe(III)-TSPP, although D values have been reported for many other high-spin ferric porphyrins, both model compounds and heme proteins. Experimental methods include far IR spectroscopy;[59] microbalance measurements of the paramagnetic anisotropy of single crystals of ferrimyoglobin fluoride;[60] and analysis of the temperature dependence of magnetic susceptibility[61] of ESR intensities,[62] of ESR relaxation times,[63] and of hyperfine chemical shifts in heme proteins.[64] The range of the measured values is $D = 5$–$16\ \mathrm{cm}^{-1}$, and we assume that $D \geqslant 5\ \mathrm{cm}^{-1}$ for bisaqua-Fe(III)-TSPP as well. The conclusion that D is large is also supported by a Mossbauer measurement[65] of the nuclear quadrupole coupling constant (e^2qQ) of Fe(III)-TSPP$\cdot 2H_2O$, which is atypically large relative to the values for other ferric porphyrins [the quantities (e^2qQ) and D are usually thought to scale with each other,[66] although the quantitative relationship is not simple]. For D the order of several wave numbers, the electron-spin system remains in the vicinity of the zfs limit throughout the range of field variation of the MRD experiment ($B_0 < 2$ T). (As a point of comparison, the intermediate regime of field strengths is located roughly where $2\omega_D/\omega_S \approx 1$. If $D = 5\ \mathrm{cm}^{-1}$ and $B_0 = 1$ T, $2\omega_D/\omega_S = 10.7$.)

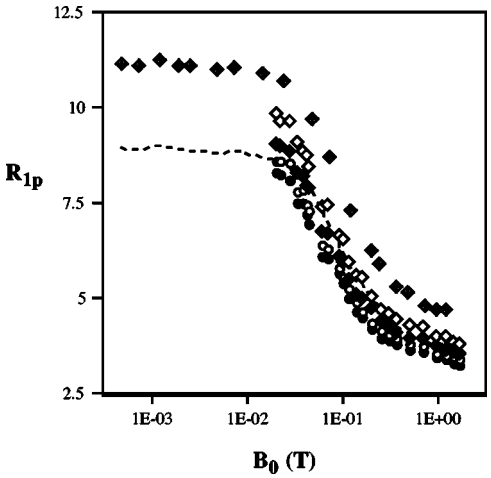

FIG. 11. R_{1p} MRD profiles (20 °C) of Fe(III)-TSPP at four pH values: pH 1, unfilled diamonds; pH 2, filled diamonds; pH 3, unfilled circles; and pH 4, filled circles. Also shown are the data from Ref. 42 (diamonds with cross) and the same data, multiplied by the factor of 0.80 (dashed line).

A. Experimental results

R_{1p} MRD profiles for Fe(III)-TSPP were measured at pH 1, 2, 3, and 4 (Fig. 11). In an earlier study, Koenig, Brown, and Spiller[67] (KBS) measured the MRD profile at pH 3 (shown as diamonds). There is a systematic variation of about 20% between our pH 3 data and that of KBS, which seems too large to attribute to differences in composition. We suspect for the following reason that systematic error is present in the KBS data. In the same study, KBS report the MRD profile of Mn(III)-TSPP, which has since been repeated by Kellar and Foster,[68] Bryant and co-workers,[5,69–71] as well as in our own laboratory.[2] A comparison of these data shows good agreement among the groups except for the profile of KBS, which is about 20% higher, as was found also for the Fe(III)-TSPP data relative to ours. Scaling the KBS data by a constant factor of 0.80 brings their data into agreement with ours (dashed line in Fig. 11).

At millimolar concentrations with pH $\leqslant 4$, Fe(III)-TSPP exists predominantly as a hexacoordinate bisaqua complex,[72] in which the Fe(III) ion is high spin ($S = 5/2$). This species deprotonates near $pK_a \approx 7$.[73] At pH $\geqslant 5$, Fe(III)-TSPP dimerizes as an antiferromagnetically coupled μ-oxobridged species.[65,74] The possible presence of dimers or noncovalent aggregates in our samples was examined by UV-vis. Spectra obtained at concentrations of 1.0 mM and 10 μM in aqueous buffers at pH 1–4 were essentially identical, indicating that neither dimerization or aggregation occurred. Spectral changes characteristic of μ-oxodimerization[75] were observed at pH $\geqslant 5$.

In order to find conditions where only the bisaqua species contributes to the NMR-PRE, we measured R_{1p} MRD profiles at integral pH values between pH 1 and 4 (Fig. 11). The shapes of the profiles are nearly constant across this pH

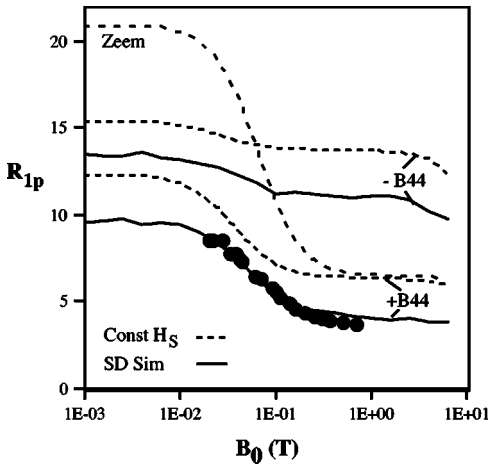

FIG. 12. Simulation of the experimental data for Fe(III)-TSPP at pH 3 (filled circles). The best-fit SD simulation is the solid curve marked +B44. Also shown is the SD simulation with the same parameters but with $\tilde{B}_4^4$ set to zero (−B44). The dashed curves were calculated in the constant H_S approximation.

range, as is the magnitude of NMR-PRE, although there is a significant (10%–15%) rise in relaxivity at pH 1 relative to pH 3–4. As the pH is raised above pH 4, the proton relaxivity falls to a low value (not shown). The constancy in shape and magnitude of the MRD profiles measured at pH 2–4 indicates that a single species, which we assume to be bisaqua Fe(III)-TSPP, is responsible. The profile measured at pH 3, after correction for the diamagnetic background, was used in the data analysis.

B. Analysis of data

The corrected data are shown in Fig. 12. The solid line labeled "+B44" shows the best SD simulation, which used the parameter set of Table I. Two parameters were varied, namely, τ_S and the ratio of zfs coefficients, $\tilde{B}_4^4/D$. The other parameters are reasonably well known from prior experiments and were assigned to the values in the table. The outer sphere contribution, $R_{1,\mathrm{os}}$, was calculated in another set of SD simulations, using MD to estimate the distance of closest approach.[76,77] $R_{1,\mathrm{os}}$ was estimated to be 2%–5% of R_{1p} and was neglected.

TABLE I. Parameters used in the simulations.

Fixed parameters	Varied parameters
$D=10\ \mathrm{cm}^{-1}$	$\tilde{B}_4^4/D=0.10$
$\tau_{R,\perp}^{(2)}=520$ ps (20 °C)[a]	$\tau_{S,r}=110$ ps (20 °C)
$\tau_M=71$ ns (25 °C)[b]	
$r_{IS}=0.275$ nm[c]	
$\theta_{IS}=0.30$ rad[c]	

[a]Reference 6, corrected for anisotropic reorientation as described in Ref. 2.
[b]Reference 83, measured by $H_2{}^{17}O$ T_2 at 25 °C. Also note that Ref. 84 reported a longer value of $\tau_M=500$ ns.
[c]Value estimated from the measured Fe–O bond distance (2.01±0.02 Å) in $Fe(H_2O)_6^{3+}$, which has been determined in solution by extended x-ray-absorption fine structure (EXAFS) (Ref. 85) and x-ray diffraction (Refs. 86 and 87) as well as from x-ray crystal structures (see Ref. 88). The Fe–O distance was assumed to be 0.10 Å longer in Fe(III)-TSPP than in $Fe(H_2O)_6^{3+}$, as has been observed for Mn(II)-TSPP.

The experimental MRD profile does not exhibit a high-field dispersive feature of the kind expected (e.g., dashed curves of Fig. 6) if τ_S was magnetic-field dependent, and thus τ_S was assumed to be magnetic-field independent in the analysis. The best-fit value, $\tau_S=110$ ps, is consistent with the results of recent pulsed ESR relaxation-time measurements[56] of Fe(III)-TSPP in frozen aqueous solutions.

As described in the previous section, the critical zfs parameter of the analysis is the mixing ratio, $\tilde{B}_4^4/D$. The shape of the MRD profile is nearly independent of the absolute value of D (assuming that D is reasonably large, $\geqslant 5\ \mathrm{cm}^{-1}$), $\tilde{B}_4^0$, or $\tilde{B}_4^4$. Omission of the $(\tilde{B}_4^4/D)$ parameter in the simulations produced an unacceptably small dispersive feature, similar to that of the model calculations of Figs. 5 and 6.

Figure 12 also shows a comparison of constant H_S calculations (dashed) and SD simulations (solid lines). As described above, constant H_S is an intermediate level of theory that accounts for Brownian reorientation of the interspin vector, $\vec{r}_{IS}$, while assuming that H_S is time independent as in a powder. Clearly, the difference between constant H_S and SD is substantial, even though $\tau_R^{(2)}$ is relatively long. Our experience in these and other simulations[44] is that in the vicinity of the zfs limit, constant H_S accounts for roughly half the effect of Brownian reorientation. A portion of this difference arises from the zfs reorientational mechanism of electron-spin relaxation.

VI. DISCUSSION

This study, like our prior investigations of aqueous metalloporphyrins of Cr(III),[3] Mn(II),[4] and Mn(III),[1,2] has found several unexpected aspects in the relationship of the spin level diagram to the MRD experiment. Fe(III)-TSPP is a spin system with $S=5/2$ and a moderately large zfs ($D>5\ \mathrm{cm}^{-1}$). The MRD profile exhibits a single pronounced Zeeman-type dispersive feature, the amplitude of which is determined by the ratio of zfs parameters, $\tilde{B}_4^4/D$. The NMR relaxation mechanism involves $\tilde{B}_4^4$-induced wave-function mixing and is specific to Kramers spin systems with $S\geqslant 5/2$ (fourth-order zfs tensor components vanish for $S=3/2$).

It is not altogether clear at this point whether this mechanism might also be important for the $S=5/2$ ion, Mn(II), and the $S=7/2$ ion, Gd(III), although for those ions D is usually much smaller than in Fe(III)-TSPP. When D is small, the permanent zfs influences the MRD profile primarily due to the change in spatial quantization which occurs in the intermediate regime ($H_{\mathrm{Zeem}}\approx H_{\mathrm{zfs}}^{\circ}$); i.e., the midfield dispersive feature in Fig. 5 occurs in a region of relatively low-field strengths that is observed in the MRD experiment. In this situation [of which Mn(II)-TSPP is an example], D, rather than the $\tilde{B}_4^4/D$ ratio, is the sensitive zfs parameter. Analyses of other Mn(II) (Refs. 78–80) and Gd(III) (Ref. 81) complexes with relatively small D values and lower symmetry than Mn(II)-TSPP have likewise suggested that D, even when small ($\leqslant 0.05\ \mathrm{cm}^{-1}$), has a significant influence in the low-field region of the MRD profile. Whether $\tilde{B}_4^4$-induced wave-function mixing is also important in Gd(III) or Mn(II) complexes needs study.

Mn(III)-TSPP is an $S=2$ spin system with a moderately large zfs ($D=-3.16\ \mathrm{cm}^{-1}$).[82] The MRD profile likewise depends on $\tilde{B}_4^4$, although the physical mechanism is quite different for the Kramers ($S=5/2$) and non-Kramers ($S=2$) systems. The former results from $\tilde{B}_4^4$-induced mixing of the circular zfs-limit eigenfunctions, while the latter involves a $\tilde{B}_4^4$-induced splitting of the $m_S=\pm 2$ non-Kramers doublet. The small splitting of these levels produces a low-frequency oscillation in the matrix elements of $\langle \hat{S}_z \rangle$ within the $m_S=\pm 2$ manifold that suppresses the NMR-PRE. The principal dispersive feature of the experimental MRD profile for $S=2$ is caused by a change in spin wave function which occurs when the electronic Zeeman energy is comparable to the $\tilde{B}_4^4$-induced doublet splitting. For this system, the important zfs parameter is $\tilde{B}_4^4$ rather than either $\tilde{B}_4^4/D$ or D. Thus the three spin systems, Mn(III)-TSPP, Mn(II)-TSPP, and Fe(III)-TSPP, exhibit qualitatively different relaxation mechanisms which depend on different zfs parameters.

Cr(III)-TSPP is an $S=3/2$ spin system with a small zfs ($0.27\ \mathrm{cm}^{-1}$). For $S=3/2$, the fourth-order zfs terms vanish by the dimensionality of the spin system. The principal MRD for $S=2$ results from the change in spatial quantization that occurs in the intermediate regime. In this case, as for Mn(II)-TSPP, the sensitive zfs parameter is D.

Other interesting phenomena have been encountered in our analyses of the relaxation mechanisms of these metalloporphyrins. For all of these systems, electron-spin relaxation appears to be nearly magnetic-field independent for $B_0<2$ T. As shown by the calculations of Fig. 6, this behavior is expected for Fe(III)-TSPP, for which D is large, and also for Mn(III)-TSPP, for which D is likewise fairly large. However, the observed lack of field dependence in τ_S is somewhat unexpected for Cr(III)-TSPP and Mn(II)-TSPP, where D is an order of magnitude smaller. Model calculations[3] suggest that this behavior results from the combined effects of the permanent zfs and short τ_v.

ACKNOWLEDGMENTS

This material is based upon the work supported by the National Science Foundation under Grant No. CHE - 0209616.

APPENDIX

Operator equivalents in Eqs. (1) and (2), taken from Table 16, Appendix B, of Ref. 9. $\{A,B\}_S$ denotes an anticommutator.

$$O_2^0 = 3S_z^2 - S(S+1),$$

$$O_2^2 = 2^{-1}(S_+^2 + S_-^2),$$

$$O_4^0 = 35S_z^4 - 30S(S+1)S_z^2 - 25S_z^2 - 6S(S+1) + 3S^2(S+1)^2,$$

$$O_4^2 = 2^{-1}\{[7S_z^2 - S(S+1) - 5],(S_+^2 + S_-^2)\}_S,$$

$$O_4^4 = 2^{-1}(S_+^4 + S_-^4).$$

[1] S. M. Abernathy, J. C. Miller, L. L. Lohr, and R. R. Sharp, J. Chem. Phys. **109**, 4035 (1998).
[2] N. Schaefle and R. Sharp, J. Phys. Chem. A, ASAP article (2005).
[3] N. Schaefle and R. Sharp, J. Phys. Chem. A, ASAP article (2005).
[4] J. C. Miller and R. R. Sharp, J. Phys. Chem. A, **104**, 4889 (2000).
[5] L. H. Bryant, M. W. Hodges, and R. G. Bryant, Inorg. Chem. **38**, 1002 (1999).
[6] N. Bloembergen and L. O. Morgan, J. Chem. Phys. **34**, 842 (1961).
[7] Nuclear-electron hyperfine couplings also produce level splittings in the absence of a Zeeman field. These terms, which are of odd order in the electron-spin operators, are not included in Eq. (1b).
[8] A. Abragam and B. Bleaney, *Electron Paramagnetic Resonance of Transition Ions* (Dover, New York, 1986).
[9] C. Rudowicz, J. Phys.: Condens. Matter **12**, L417 (2000).
[10] S. Rast, P. H. Fries, and E. Belorizky, J. Chem. Phys. **113**, 8724 (2000).
[11] S. Rast, P. H. Fries, E. Belorizky, A. Borel, L. Helm, and A. E. Merbach, J. Chem. Phys. **115**, 7554 (2001).
[12] E. Belorizky and P. H. Fries, Phys. Chem. Chem. Phys. **6**, 2341 (2004).
[13] S. Rast, A. Borel, E. Belorizky, P. H. Fries, and A. E. Merbach, J. Am. Chem. Soc. **123**, 2637 (2001).
[14] Z. Luz and S. Meiboom, J. Chem. Phys. **40**, 2686 (1964).
[15] I. Solomon, Phys. Rev. **99**, 555 (1955).
[16] N. Bloembergen, J. Chem. Phys. **27**, 572 (1957); **27**, 595 (1957).
[17] L. Banci, I. Bertini, F. Briganti, and C. Luchinat, J. Magn. Reson. (1969-1992) **66**, 58 (1986).
[18] I. Bertini, C. Luchinat, M. Mancini, and G. Spina, J. Magn. Reson. (1969-1992) **59**, 213 (1984).
[19] N. Benetis, J. Kowalewski, L. Nordenskioeld, H. Wennerstroem, and P. O. Westlund, Mol. Phys. **48**, 329 (1983).
[20] N. Benetis, J. Kowalewski, L. Nordenskioeld, H. Wennerstroem, and P.-O. Westlund, J. Magn. Reson. (1969-1992) **58**, 261 (1984).
[21] J. Kowalewski, L. Nordenskiold, N. Benetis, and P.-O. Westlund, Prog. Nucl. Magn. Reson. Spectrosc. **17**, 141 (1985).
[22] P.-O. Westlund, H. Wennerstrom, L. Nordenskiold, J. Kowalewski, and N. Benetis, J. Magn. Reson. (1969-1992) **59**, 91 (1984).
[23] P.-O. Westlund, N. Benetis, and H. Wennerstrom, Mol. Phys. **61**, 177 (1987).
[24] T. Larsson, P.-O. Westlund, J. Kowalewski, and S. H. Koenig, J. Chem. Phys. **101**, 1116 (1994).
[25] P.-O. Westlund and P. T. Larsson, Acta Chem. Scand. **45**, 11 (1991).
[26] J. Kowalewski, C. Luchinat, T. Nilsson, and G. Parigi, J. Phys. Chem. A **106**, 7376 (2002).
[27] D. Kruk and J. Kowalewski, J. Chem. Phys. **116**, 4079 (2002).
[28] T. Nilsson, J. Svoboda, P.-O. Westlund, and J. Kowalewski, J. Chem. Phys. **109**, 6364 (1998).
[29] D. Kruk and J. Kowalewski, Mol. Phys. **101**, 2861 (2003).
[30] T. Nilsson and J. Kowalewski, J. Magn. Reson. **146**, 345 (2000).
[31] T. Nilsson and J. Kowalewski, Mol. Phys. **98**, 1617 (2000).
[32] D. Kruk, T. Nilsson, and J. Kowalewski, Phys. Chem. Chem. Phys. **3**, 4907 (2001).
[33] R. R. Sharp, J. Chem. Phys. **93**, 6921 (1990).
[34] R. R. Sharp, J. Chem. Phys. **98**, 912 (1993).
[35] R. R. Sharp, J. Chem. Phys. **98**, 6092 (1993).
[36] J.-M. Bovet and R. R. Sharp, J. Chem. Phys. **99**, 18 (1993).
[37] S. M. Abernathy and R. R. Sharp, J. Chem. Phys. **106**, 9032 (1997).
[38] R. Sharp, S. M. Abernathy, and L. L. Lohr, J. Chem. Phys. **107**, 7620 (1997).
[39] R. Sharp, L. Lohr, and J. Miller, Prog. Nucl. Magn. Reson. Spectrosc. **38**, 115 (2001).
[40] N. Schaefle and R. Sharp, J. Chem. Phys. **121**, 5387 (2004).
[41] R. Sharp, J. Magn. Reson. (1969-1992) **100**, 491 (1992).
[42] N. Schaefle and R. Sharp, J. Magn. Reson. (submitted).
[43] E. N. Ivanov, Zh. Eksp. Teor. Fiz. **45**, 1509 (1963) [Sov. Phys. JETP **18**, 1041 (1964)].
[44] J. C. Miller, N. Schaefle, and R. Sharp, Magn. Reson. Chem. **41**, 806 (2003).
[45] M. Odelius, C. Ribbing, and J. Kowalewski, J. Chem. Phys. **103**, 1800 (1995).
[46] M. Odelius, C. Ribbing, and J. Kowalewski, J. Chem. Phys. **104**, 3181 (1996).
[47] S. Fries, E. Belorizky, A. Borel, L. Helm, and A. E. Merbach, J. Chem. Phys. **115**, 7554 (2001).
[48] I. Bertini, O. Galas, C. Luchinat, and G. Parigi, J. Magn. Reson., Ser. A **113**, 151 (1995).

[49]P.-O. Westlund, Mol. Phys. **85**, 1165 (1995).
[50]R. Sharp and L. L. Lohr, J. Chem. Phys. **115**, 5005 (2001).
[51]R. Sharp, J. Magn. Reson. **154**, 269 (2002).
[52]S. A. Al'tshuler and K. A. Valiev, Sov. Phys. JETP **35**, 661 (1959).
[53]D. Kruk, J. Kowalewski, and P.-O. Westlund, J. Chem. Phys. **121**, 2215 (2004).
[54]P.-O. Westlund, J. Chem. Phys. **108**, 4945 (1998).
[55]I. Bertini, J. Kowalewski, C. Luchinat, T. Nilsson, and G. Parigi, J. Chem. Phys. **111**, 5795 (1999).
[56]Y. Zhou, B. E. Bowler, G. R. Eaton, and S. Eaton, J. Magn. Reson. **144**, 115 (2000).
[57]Formulations of both SLE and MC have been developed, which are valid in the regime of slow zfs distortional motions.
[58]R. R. Sharp, J. Chem. Phys. **98**, 2507 (1993).
[59]Far IR has been used to detect the $m_S=\pm 1/2$ to $m_S=\pm 3/2$ transition in 18 high-spin ferric porphyinates with fluoro-, chloro-, iodo-, and azido ligands, as well as in ferrimyoglobin with fluoro- and aqua ligands, and in ferrihemoglobin with a fluoroligand; P. L. Richards, W. S. Caughey, H. Eberspaecher, G. Feher, and M. Malley, J. Chem. Phys. **47**, 1187 (1967); G. C. Brackett, P. L. Richards, and W. S. Caughey, *ibid.* **54**, 4383 (1971); G. Feher and P. L. Richards, *Proceeding of the Second International Conference on Magnetic Resonance in Biological Systems*, Wenner-Gren Center, Stockholm, June 1966 (Pergamon Press, New York, 1967), p. 141.
[60]H. Uenoyama, T. Hzuka, H. Morimoto, and M. Kotoni, Biochim. Biophys. Acta **160**, 159 (1968).
[61]G. Lang, B. Boso, B. S. Erler, and C. A. Reed, J. Chem. Phys. **84**, 2998 (1986).
[62]E. L. Bominaar, X.-Q. Ding, A. Gismelseed, E. Bill, H. Winkler, A. X. Trautwein, H. Nasri, J. Fischer, and R. Weiss, Inorg. Chem. **31**, 1845 (1992).
[63]In ferric porphyrins, the low-temperature electron-spin relaxation mechanism contains a strong Orbach contribution, from which the $m_S=\pm 1/2$ to $m_S=\pm 3/2$ doublet splitting has been inferred; C. P. Scholes, R. A. Isaacson, and G. Feher, Biochim. Biophys. Acta **244**, 206 (1971); Y. Zhou, B. E. Bowler, G. R. Eaton, and S. Eaton, J. Magn. Reson. **144**, 115 (2000).
[64]K. Clark, L. B. Dugad, R. G. Bartsch, M. A. Cusanovich, and G. N. La Mar, J. Am. Chem. Soc. **118**, 4654 (1996); A. Asokan, J. S. de Ropp, S. L. Newmyeer, P. R. Ortiz de Montellano, and G. N. La Mar, *ibid.* **123**, 4243 (2001); P. Tsan, M. Caffrey, M. L. Daku, M. Cusanovich, S. Marion, and P. Gans, *ibid.* **123**, 2231 (2001).
[65]J. Silver and B. Lukas, Inorg. Chim. Acta **92**, 259 (1984).
[66]C. Maricondi, D. K. Straub, and L. M. Epstein, J. Am. Chem. Soc. **94**, 4157 (1972).
[67]S. H. Koenig, R. D. Brown, and M. Spiller, Magn. Reson. Med. **4**, 252 (1987).
[68]K. E. Kellar and N. Foster, Inorg. Chem. **32**, 1353 (1992).
[69]G. Hernandez and R. G. Bryant, Bioconjugate Chem. **2**, 394 (1991).
[70]J. E. Bradshaw, K. A. Gillogly, L. J. Wilson, K. Kumar, X. Wan, M. F. Tweedle, G. Hernandez, and R. G. Bryant, Inorg. Chim. Acta **275–6** 106 (1998).
[71]S. Sur and R. G. Bryant, J. Phys. Chem. **99**, 4900 (1995).
[72]P. Hambright, *Chemistry of Water Soluble Porphyrins* in The Porphyrin Handbook Vol. 3, edited by K. M. Kadish, K. M. Smith, and R. Guilard (Academic, New York, 2000), Chap. 18.
[73]A. A. El-Awady, P. C. Wilkins, and R. G. Wilkins, Inorg. Chem. **24**, 2053 (1985).
[74]H. Goff and L. O. Morgan, Inorg. Chem. **15**, 3180 (1976).
[75]A. A. El-Awady, P. C. Wilkins, and R. G. Wilkins, Inorg. Chem. **24**, 2053 (1985).
[76]J. C. Miller, S. M. Abernathy, L. L. Lohr, and R. R. Sharp, J. Phys. Chem. A **104**, 9481 (2000).
[77]J. C. Miller, L. L. Lohr, and R. R. Sharp, J. Magn. Reson. **148**, 267 (2001).
[78]E. Strandberg and P.-O. Westlund, J. Magn. Reson. **137**, 333 (1999).
[79]D. Kruk and J. Kowalewski, JBIC, J. Biol. Inorg. Chem. **8**, 512 (2003).
[80]S. Aime, P. L. Anelli, M. Botta, M. Brocchetta, S. Canton, F. Fedeli, E. Gianoio, and E. Terreno, JBIC, J. Biol. Inorg. Chem. **7**, 58 (2002).
[81]X. Zhou, P. Caravan, R. B. Clarkson, and P.-O. Westlund, J. Magn. Reson. **167**, 147 (2004).
[82]J. Krzystek and J. Telser, J. Magn. Reson. **162**, 454 (2003).
[83]I. J. Ostrich, G. Liu, H. W. Dodgen, and J. P. Hunt, Inorg. Chem. **19**, 619 (1980).
[84]T. Schneppensieper, A. Zahl, and R. v. Eldic, Angew. Chem., Int. Ed. **40**, 1678 (2001).
[85]K. Asakura, M. Nomura, and H. Kuroda, Bull. Chem. Soc. Jpn. **58**, 1542 (1985).
[86]M. Magini and R. Caminiti, J. Inorg. Nucl. Chem. **39**, 91 (1977).
[87]M. Magini, J. Chem. Phys. **70**, 317 (1979).
[88]M. Montgomery, R. V. Chastain, and E. C. Lingafelter, Acta Crystallogr. **20**, 731 (1966).